



Isomer effect of propanol on liquid–liquid equilibrium in hydrophobic room-temperature ionic liquids



Shinichiro Ozawa^a, Hiroaki Kishimura^a, Shota Kitahira^a, Kentaro Tamatani^a, Kentaro Hirayama^a, Hiroshi Abe^{a,*}, Yukihiro Yoshimura^b

^a Department of Materials Science and Engineering, National Defense Academy, Yokosuka 239-8686, Japan

^b Department of Applied Chemistry, National Defense Academy, Yokosuka 239-8686, Japan

ARTICLE INFO

Article history:

Received 2 May 2014

In final form 1 September 2014

Available online 6 September 2014

ABSTRACT

The cloud-point temperature determined the liquid–liquid phase equilibrium (LLE) of binary systems comprising hydrophobic room-temperature ionic liquids (RTILs) and propanol. The RTILs were 1-alkyl-3-methylimidazolium bis(trifluoromethanesulfonyl)imide, $[C_xmim][TFSI]$ ($2 \leq x \leq 10$). Upper critical solution temperatures in LLE are inversely proportional to the C_xmim^+ cation alkyl chain length, x . The propanol isomer effect indicates the critical alkyl chain length ($x_{critical} = 6–7$). UNIQUAC model determined the interaction parameters (with crossing points at $x = 6$). In pure RTILs, conformation stability of $TFSI^-$ by Raman spectroscopy changed between $x = 6$ and 7, corresponding to the simulation-determined 90°-torsion angle at $x = 6$.

© 2014 Elsevier B.V. All rights reserved.

1. Introduction

Room-temperature ionic liquids (RTILs) are widely applied in the fields of green chemistry such as CO_2 capture and separation technology [1–5]. Moreover, the RTILs are utilized as a recyclable solvent. The latter use consists of a purification process under vacuum utilizing a nearly zero vapor pressure of the RTILs. The high cost of the RTILs is major barrier for its wide-spread use. Thus, pure RTILs have to be replaced with alcohol-diluted ones for industrial applications that use fair amounts of RTILs.

Liquid phase stability in RTIL-based binary and ternary solutions is well examined from a fundamental thermodynamic point of view [6–11]. This knowledge is indispensable for designing and optimizing chemical engineering processes in real industrial systems. For new molecular designing based on large numbers of cation/anion combinations, the databanks using group contribution methods are useful for predicting solution properties [12–15]. Through the efforts of many researches, many kinds of liquid–liquid equilibrium (LLE) were determined, and the types of molecular interactions were classified based on thermodynamic models. These models contain molecular structures and activity coefficients in the solutions. Representative computer-aided models are the universal functional activity coefficient (UNIFAC) [16,17] and the universal quasichemical (UNIQUAC) [18–20] models. The LLE in

RTIL-based binary and ternary mixtures is well described by the models combined with density functional theory (DFT). Furthermore, the UNIQUAC method was applied on the pressure scale for CO_2 capture and separation [21].

Bis(trifluoromethanesulfonyl)imide anion ($TFSI^-$) has two stable conformers: *cis* (C_1) and *trans* (C_2). The isomerism of $TFSI^-$ anion is a key to understand the phase stability in liquid [22,23], low temperature [24] and high pressure [25] amorphous, and crystalline [26,27] forms. For instance, the conformational stability of 1-ethyl-3-methylimidazolium cation (C_2mim^+) and $TFSI^-$ anion are evaluated by DFT calculations [22–24]. Here, x in C_xmim^+ indicates the alkyl chain length. C_1 and C_2 conformers of the $TFSI^-$ anion are quite sensitive to the molecular packing and the local circumstances. Furthermore, combined with *n*-alkyl alcohols, $C_nH_{2n+1}OH$, LLEs of $[C_1mim][TFSI]$ [28], $[C_2mim][TFSI]$ [29], $[C_3mim][TFSI]$ [28], $[C_4mim][TFSI]$ [30] and $[C_6mim][TFSI]$ [31] are examined in detail. Universal curve was obtained by the reduced UCSTs and critical mole fraction, x_c .

In this study, we investigated liquid phase stabilities of $[C_xmim][TFSI]$ -propanol, considering the alkyl chain length, propanol isomer effect, and $TFSI^-$ conformers. To understand mutual solubility on the molecular level, we calculate the UNIQUAC interaction parameters obeying quantum chemistry.

2. Materials and methods

The RTILs used in this study are hydrophobic $[C_xmim][TFSI]$ ($x = 2–10$) (IoLiTec GmbH and Kanto Chemical Co.). As propanol

* Corresponding author.

E-mail address: ab@nda.ac.jp (H. Abe).

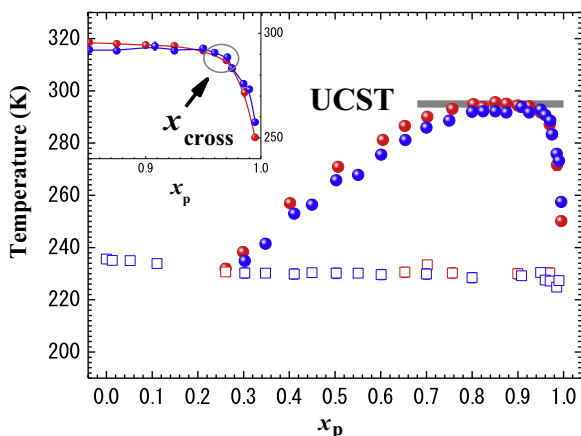


Figure 1. T - x_p phase diagram of 1-ethyl-3-methylimidazolium bis(trifluoromethylsulfonyl)imide, $[\text{C}_2\text{mim}][\text{TFSI}]$ and propanol system, showing upper critical temperature (UCST). Red and blue closed circles reveal the cloud-point temperatures of 1- and 2-propanol-based mixtures, respectively. The enlarged phase diagram in the inset of figure indicates the intersecting curves at the crossing concentration, x_{cross} . Crystallization temperatures of 1- and 2-propanol-based mixtures are expressed by red and blue open squares, respectively. (For interpretation of the references to color in this figure legend, the reader is referred to the web version of this article.)

acts as additives for the mixtures, we used 1-propanol (99.5%) and 2-propanol (99.5%) (Kanto Chemical Co.). Further information is provided in Supporting information.

To determine the LLE at ambient pressure, the mixtures were cooled from 303 K down to 203 K using an ethanol bath (Yamato Scientific Co., BE200); thus, at this point, clouding of the mixtures was visually observed. By visual cloud-point determinations, accuracy of the clouding temperatures was found to be within 0.5 K. Several thermal cycles using the same sample and measurements using different samples at the same concentration can determine the experimental errors of the clouding temperatures. A liquid N_2 pot was used as a supplement for further cooling [32]. Temperature was monitored by a Pt100 (Netsushin Co.). The cooling rate was 1.5 K/min.

Conformation stabilities in the mixtures were examined by Raman spectroscopy. Raman spectra were measured in a backscattering geometry using a micro-Raman spectrometer (NR-1800, JASCO Co.) equipped with a single monochromator and a CCD detector. The 514.5 nm/line from a Lexel Ar⁺ ion laser was used as an excitation source with a power of 250 mW. Raman spectra were measured at room temperature and ambient pressure.

3. Results and discussion

3.1. Propanol isomer effect in liquid–liquid equilibria

LLE data for $[\text{C}_2\text{mim}][\text{TFSI}]$ - x_p mol% propanol were obtained from the clouding temperature (Figure 1). Actual dataset of the clouding temperature is listed in Table S2 for Supporting information. Red closed circles and open squares in the figure indicate the clouding and crystallization temperatures of 1-propanol-based mixtures, respectively. Blue circles and squares show those of 2-propanol-based mixtures. The reproducibility of visual detection of liquid–liquid immiscibility was within ± 0.5 K. On cooling, $[\text{C}_2\text{mim}][\text{TFSI}]$ -propanol crystallized over a wide range of propanol concentration. In Figure 1, the crystallization temperatures are represented by open squares. In a previous study [26], however, by using differential scanning calorimetry (DSC), no phase changes of pure $[\text{C}_2\text{mim}][\text{TFSI}]$ were observed on cooling, although cold crystallization occurred on heating. In another study [27], an exothermal peak of pure $[\text{C}_2\text{mim}][\text{TFSI}]$ was observed at 222 K on

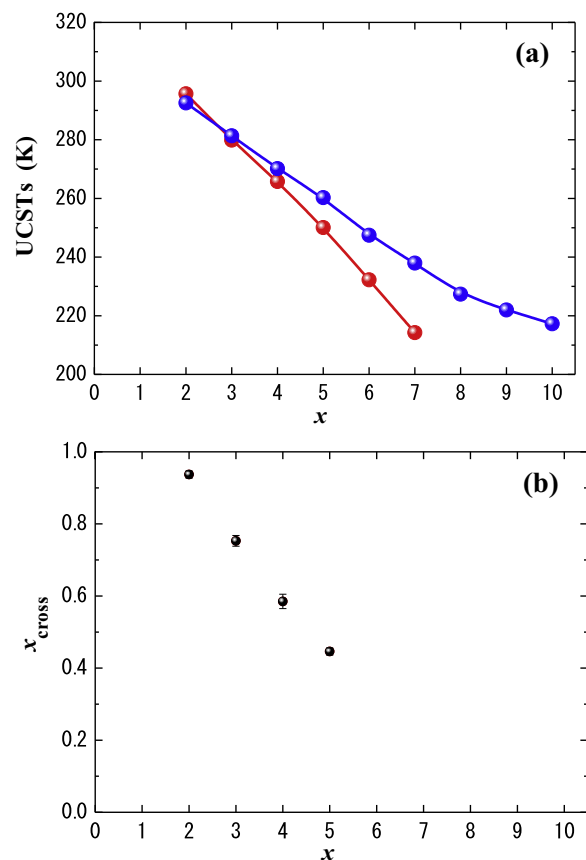


Figure 2. Alkyl chain length, x , dependence of (a) upper critical solution temperatures (UCSTs) and (b) cross concentration, x_{cross} . Red and blue closed circles in Figure 3(a) correspond to the UCSTs of 1- and 2-propanol-based mixtures. (For interpretation of the references to color in this figure legend, the reader is referred to the web version of this article.)

the cooling DSC thermograph (cooling rate: 10 K/min). On cooling, the amorphization and crystallization of pure $[\text{C}_2\text{mim}][\text{TFSI}]$ are quite sensitive to the experimental conditions. Although pure $[\text{C}_2\text{mim}][\text{TFSI}]$ is unstable, propanol-based mixtures have reproducible clouding temperatures on cooling. In the LLE, two significant properties of the propanol isomer effect are denoted by the arrows in Figure 1. One is the appearance of a crossing point (x_{cross}) in the clouding temperature curves in the propanol-rich region as shown in the inset of Figure 1. The other is the observation of small different upper critical solution temperatures (UCSTs) in $[\text{C}_2\text{mim}][\text{TFSI}]$ -1-propanol and -2-propanol mixtures.

In order to clarify the C_xmim^+ cation-dependent isomer effect of 1-propanol and 2-propanol, Figure 2(a) shows the UCSTs plotted against the alkyl chain length ($x = 2$ –10). In Supporting information, T - x_p plots (Figure S1) and data of the clouding temperatures (Table S2) are summarized. In each mixture, the side chain effect described by x is characterized by a monotonic decrease in the UCSTs. At $x > 7$, clouding temperatures of 1-propanol-based mixtures were not observed at all, because the UCSTs are lower than the experimental minimum temperature (203 K). The propanol isomer effect results in increased differences in the UCSTs with increasing x . The contradictory behavior of the UCSTs suggests that the propanol isomer effect is enhanced under larger nanodomains. Pure $[\text{C}_x\text{mim}][\text{TFSI}]$ ($x = 2$ –10) is well known to develop nanoheterogeneities at room temperature develop with increasing n because of the growth of polar and non-polar nanodomains [33]. Additionally, the melting points of the pure system are affected by the nanoheterogeneities that depend on x . The melting points of $[\text{C}_x\text{mim}][\text{TFSI}]$ ($x = 2$ –10) decrease proportionally with x [34]. Both the larger nanodomains

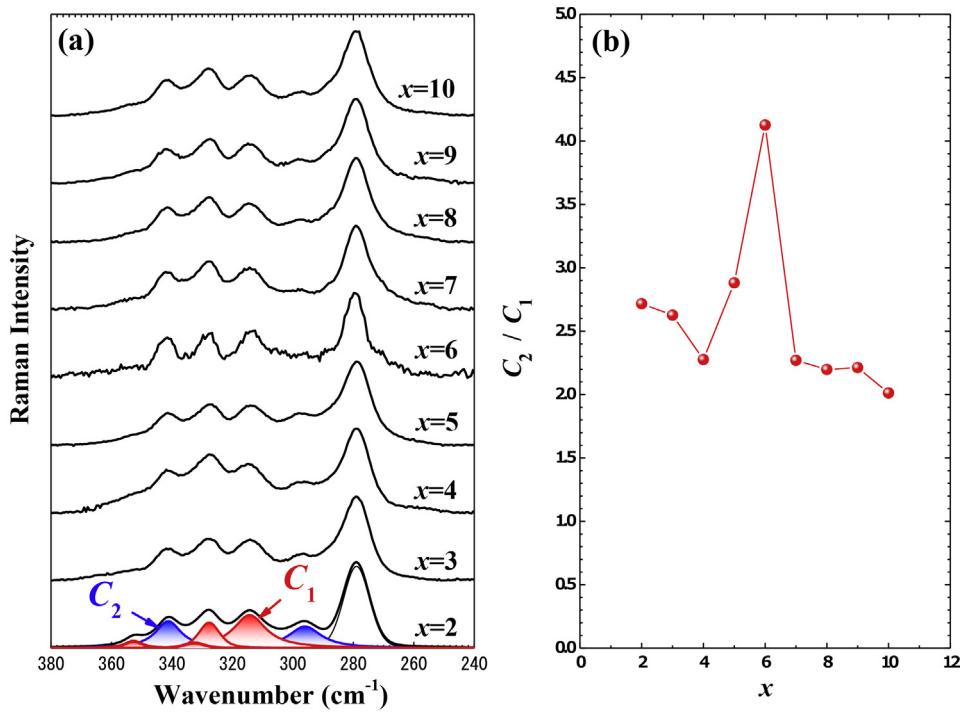


Figure 3. (a) Raman spectra of pure $[C_x\text{mim}][\text{TFSI}]$ ($x=2–10$) and (b) alkyl chain length, x , dependence of the intensity ratio between the C_1 and C_2 conformers of TFSI^- anion. Decomposed peaks in Figure 3(a) profiles are assigned as C_1 and C_2 conformers of TFSI^- anion, referring to the previous studies [22–24].

and the lower melting points in the pure system have relationships with decreasing UCSTs in the $[C_x\text{mim}][\text{TFSI}]$ -propanol system that are proportional to x . As mentioned previously, in Figure 1, x_{cross} is significant for liquid phase stability as well as for the UCSTs. Figure 2(b) shows x_{cross} as a function of x . Due to the experimental limitations on cooling, x_{cross} at $x > 5$ was not observed. With an increase in x , x_{cross} shifts to lower concentrations. The clouding at x_{cross} indicates that the inherent coordination number of propanol controls the clouding at the same temperature in spite of the geometrically-different structures of 1-propanol and 2-propanol. The isomer effect in the solutions disappears only at x_{cross} . Molecular dynamics (MD) simulations predict the molecular interactions among $C_x\text{mim}^+$, Cl^- and 1-propanol. Simulations of $[C_x\text{mim}][\text{Cl}]$ ($x=2, 4$, and 6)-1-propanol demonstrate that for $x=6$, Cl^- anion is bound to 1-propanol by hydrogen bonding [35].

3.2. Raman spectroscopy

Based on the MD simulation results [35] that suggest the molecular interaction between Cl^- anion and propanol, we speculate that the TFSI^- anion has some relationship with propanol. The contribution of the TFSI^- anion in pure $[C_x\text{mim}][\text{TFSI}]$ system was investigated with Raman spectroscopy. Raman spectra of pure $[C_x\text{mim}][\text{TFSI}]$ ($x=2–10$) at room temperature (295 K) are shown in Figure 3(a). C_1 and C_2 conformers of the TFSI^- anion are assigned in the wavenumber region from 240 to 380 cm^{-1} [32]. The spectrum of $[C_2\text{mim}][\text{TFSI}]$ is exactly the same as that reported by a previous study [24]. In the same manner with the previous study [25], peak separation and assignments are performed considering C_1 and C_2 conformers of the TFSI^- anion. The bottom spectrum in Figure 3(a) of the pure $[C_2\text{mim}][\text{TFSI}]$ is revealed as the representative decomposed Raman bands. For a quantitative estimation depending on x , a conformational stability of the TFSI^- anion is analyzed. Intensity fraction of C_2/C_1 is shown in Figure 3(b). A significant finding is that the C_2/C_1 varies discretely between $x=6$ and $x=7$. This implies that TFSI^- anion is not stabilized by the specific alkyl chain length ($x=6–7$). Thus, we define the critical alkyl chain length as x_{critical} .

Nanoheterogeneity in pure $[C_x\text{mim}][\text{TFSI}]$ ($x=2–10$) was examined [33]. An additional peak in the small q region of the X-ray diffraction patterns appeared because of the longer alkyl chain ($x=6–10$). The size of the nanodomain was reported to be proportional to x , where the relation was described as $0.196x + 0.312$ (nm). Considering the peak appearance above $x=6$, $[C_6\text{mim}][\text{TFSI}]$ is considered to possess a crossover chain length. For further understanding, DFT calculations are indispensable to interpret the above experimental results. DFT calculations, even in the gas phase, might provide a hint to resolve experimental data on the molecular level. In the pure $[C_x\text{mim}][\text{TFSI}]$ ($x=1–12$) system, DFT calculations were performed using the Lee–Yang–Pee correlation (B3LYP) 6–31+G(d,p) basis set [36,37] with the PC-GAMESS package [38]. A significant finding is that the torsional angle, α , of TFSI^- changes drastically at $x=6$ in pure $[C_x\text{mim}][\text{TFSI}]$ (Figure 4(b)). The torsional angle of C–S–S–C is defined as shown in Figure 4(a). In the gas phase (one pair of cation and anion), the torsional angle depends extensively on x , for instance, at $x < 6$, the C_1 conformer of TFSI^- is preferred in the gas state. In contrast, the C_2 conformer appears in the simulation box when at $x > 6$. Thus, $[C_6\text{mim}][\text{TFSI}]$ is found to express a crossover state from C_1 to C_2 conformers. The DFT calculations suggest that $[C_6\text{mim}][\text{TFSI}]$ is energetically unstable in the gas phase. Hence, we suppose that the singular $x=6$ in the simulations is related to the discrete jump of C_2/C_1 at $x_{\text{critical}}=6–7$, which is clarified by the analysis of the observed Raman spectra. Here, we emphasize that, in the simulations, one molecule of TFSI^- is merely optimized energetically, although so many C_1 and C_2 TFSI^- molecules coexist in real system. Apart from quantitative estimations, a discontinuous point at $x=6$ in the experiments and simulations is responsible for the conformation stability of TFSI^- .

3.3. Upper critical solution temperatures of *n*-alkyl alcohol-based mixtures

Previously, effects of alkyl chain length of *n*-alkyl alcohol as additives were investigated in $[C_x\text{mim}][\text{TFSI}]$ ($x=1, 2, 3, 4$ and 6). A series of the *n*-alkyl alcohols is 1-propanol ($n=3$),

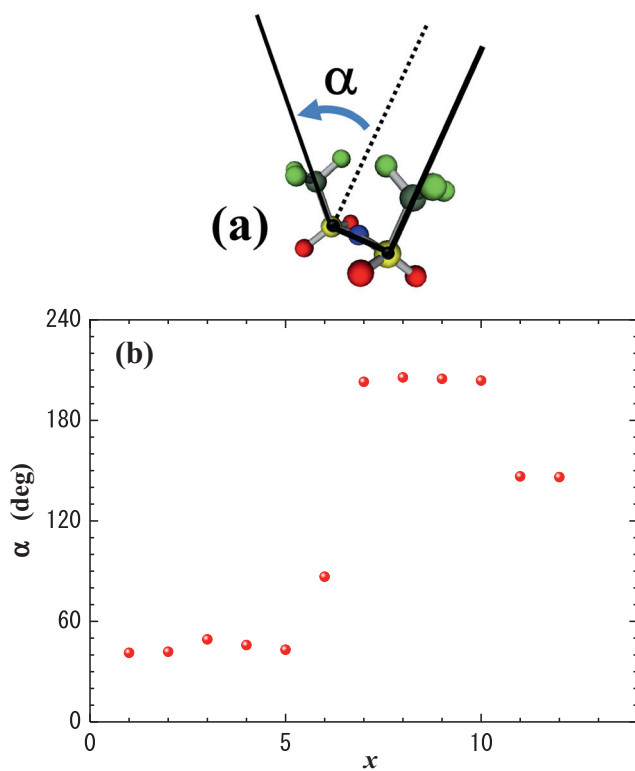


Figure 4. (a) Definition of torsional angle, α , ($C-S-S-C$) in $TFSI^-$ anion, (b) the torsional angle of $TFSI^-$ as a function of alkyl chain length, x , on the basis of the B3LYP/6-31++G(d,p). The torsional angle changes discontinuously at $x=6$.

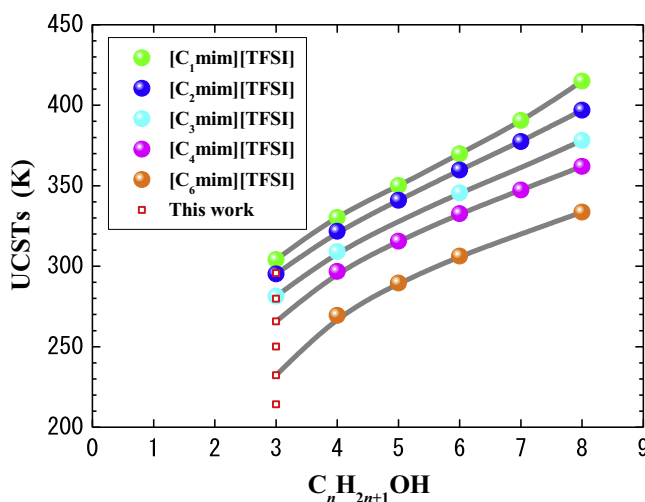


Figure 5. UCSTs in $[C_xmim][TFSI]-C_nH_{2n+1}OH$ system. Closed circles reveal the UCSTs determined by the previous works [28–31]. Our results ($2 \leq x \leq 7$ and $n=3$) are expressed by open squares. A rapid decrease at around $n=3$ is enhanced in the $[C_3mim][TFSI]$ -based mixture.

1-butanol ($n=4$), 1-pentanol ($n=5$), 1-hexanol ($n=6$), 1-heptanol ($n=7$) and 1-octanol ($n=8$). By the LLE determinations, UCSTs of $[C_xmim][TFSI]-C_nH_{2n+1}OH$ system were obtained in Figure 5 [28–31]. Combined with the previous results, the UCSTs of our results are plotted by open squares, where the mixtures are $[C_xmim][TFSI]$ -1-propanol ($2 \leq x \leq 7$ and $n=3$). Our data (open squares) coincide with the previous one within experimental errors. In the $[C_xmim][TFSI]-C_nH_{2n+1}OH$ system, the UCST increases with increasing n .

Table 1

van der Waals volume (V) and surface area (A) calculated by PC-GAMESS. Volume (r) and surface area (q) structural parameters are obtained using V and A (see text).

	V \AA^3	A \AA^2	r	q
$[C_2mim][TFSI]$	266.155	344.526	10.5673	8.3003
$[C_3mim][TFSI]$	283.215	367.644	11.2446	8.8573
$[C_4mim][TFSI]$	300.040	389.418	11.9126	9.3819
$[C_5mim][TFSI]$	316.927	411.273	12.5831	9.9084
$[C_6mim][TFSI]$	334.501	437.469	13.2808	10.5395
$[C_7mim][TFSI]$	351.759	457.617	13.9660	11.0249
$[C_8mim][TFSI]$	368.118	476.594	14.6155	11.4821
$[C_9mim][TFSI]$	383.834	496.428	15.2395	11.9599
$[C_{10}mim][TFSI]$	399.966	517.963	15.8800	12.4788
1-Propanol	70.519	103.179	2.7998	2.4858
2-Propanol	70.439	102.993	2.7967	2.4813

Our experimental results in the 1-propanol-based mixtures ($2 \leq x \leq 7$ and $n=3$) suggest that UCSTs have no linear relationship with the alkyl chain length of n -alkyl alcohols. In particular, the UCST of the $[C_6mim][TFSI]$ -based mixture is described by a sudden decrease at $n=3$ (Figure 5). This tendency might be enhanced by larger x and smaller n . We suppose that the most enhanced non-linearity at $x=6$ has some relation with previously defined critical alkyl chain length as x_{critical} (=6–7). At least, molecular interactions among cation, anion and alcohols are not so simple in the $[C_xmim][TFSI]-C_nH_{2n+1}OH$ system, where solubility is much promoted by a combination of large x or small n .

4. Simulations using the UNIQUAC equation

4.1. UNIQUAC activity coefficient model

UNIQUAC was developed from the quasichemical theory of non-ideal solutions as one of the thermodynamic models for calculating activity coefficient. The UNIQUAC model is introduced semi-empirically [39,40]. The activity coefficient of the i -component, γ_i , is given by,

$$\ln \gamma_i = \ln \gamma_i^C + \ln \gamma_i^R, \quad (1)$$

where γ_i^C is a combinatorial part representing pure i -molecule size and shape effects, and γ_i^R is a residual expressing intermolecular forces (mixing enthalpy). The first term in Eq. (1) contains the structural volume parameter, r_i , and surface area parameter, q_i , for the pure component. The second term consists of q_i and the UNIQUAC interaction parameters, a_{ij} , which reveal the parameterized energy of the $i-j$ interactions. Detailed relations among the parameters are described in the references [16–20,39,40]. In a_{ij} , the i -molecule is at origin with the j -molecules surrounding it. If a_{ij} is positive, the j -th molecule surrounding the central one is not preferred. In contrast, the $i-j$ interaction is attractive when a_{ij} is negative. To quantitatively estimate r_i and q_i in binary systems (Table 1), we performed DFT calculations of pure RTILs and additives in the gas state using the B3LYP, 6-31++G(d,p) basis set [36,37].

4.2. UNIQUAC interaction parameters

Generally, using the LLE, UNIQUAC parameters indicating intermolecular interactions are obtained semi-empirically as described in the previous section. Subscripts 1 and 2 of a_{12} correspond to the RTILs and propanol, respectively. The calculated a_{12} and a_{21} are listed in Table 2; the values are calculated only by LLEs that contain enough data points (>10). The calculations are optimized by a convergent condition, S (see Supporting information). The a_{ij}

Table 2UNIQUAC interaction parameters, a_{12} and a_{21} . Subscript 1 and 2 reveal the RTIL and propanol, respectively.

	1-Propanol			2-Propanol		
	a_{12}	a_{21}	δ_{xp}	a_{12}	a_{21}	δ_{xp}
[C ₂ mim][TFSI]	570.003	−153.019	0.0757	663.003	−185.019	0.0781
[C ₃ mim][TFSI]	589.007	−165.886	0.0497	660.003	−185.019	0.0743
[C ₄ mim][TFSI]	642.116	−185.006	0.0841	667.003	−185.019	0.0967
[C ₅ mim][TFSI]	623.411	−185.001	0.0870	668.010	−202.228	0.0677
[C ₆ mim][TFSI]	659.005	−212.400	0.0399	660.037	−208.009	0.0570
[C ₇ mim][TFSI]	735.010	−257.228	0.0198	670.026	−216.541	0.0506
[C ₈ mim][TFSI]	−	−	−	792.411	−266.001	0.0504
[C ₉ mim][TFSI]	−	−	−	−	−	−
[C ₁₀ mim][TFSI]	−	−	−	−	−	−

accuracy is described by root mean square deviation, δ_{xp} . δ_{xp} is given by,

$$\delta_{xp} = \sqrt{\frac{\sum_j^M \sum_i^{N-1} \{(x_{ij}^{I,\text{exp}} - x_{ij}^{I,\text{cal}})^2 + (x_{ij}^{II,\text{exp}} - x_{ij}^{II,\text{cal}})^2\}}{2MN}}. \quad (2)$$

N and M are the number of data points of tie-lines. The molecular interactions between the RTILs and propanol are characterized by the decomposed a_{12} and a_{21} . Stronger molecular interactions are observed with increasing $C_x\text{mim}^+$ alkyl chain length. Note that all a_{12} values are positive, indicating that the RTILs are repulsive to propanol. Thus, a positive a_{12} corresponds indirectly to the attractive interaction between a cation and an anion. On the other hand, a_{21} is derived from the correlation of propanol-cation or propanol-anion. The a_{21} values of 1-propanol- and 2-propanol-based mixtures intersect at around $x=6$. Propanol-RTIL interactions described by a_{21} support the critical alkyl chain length of $x_{\text{critical}}=6\text{--}7$, which was derived from the UCST plot, the specific torsional angle at $x=6$ determined by DFT, the discrete C_2/C_1 jump at $x_{\text{critical}}=6\text{--}7$, and the development of nanodomains above $x=6$ [31]. Additionally, the positive a_{12} describing the cation–anion interactions has a crossing point at $x=6$. Depending on the propanol isomer, the cation and anion interactions are also influenced by the x_{critical} of $C_x\text{mim}^+$.

5. Summary

Critical alkyl chain length ($x_{\text{critical}}=6\text{--}7$) is determined by a series of the LLE in the $[C_n\text{mm}][\text{TFSI}]$ -propanol mixtures. Intersecting points at $x=6$ in the UNIQUAC interaction parameters reveal that the propanol isomer contribution drastically changes in the vicinity of x_{critical} . In the pure system, discontinuity of TFSI^- conformations ($x_{\text{critical}}=6\text{--}7$) corresponds to the 90°-torsional angle of TFSI^- ($x=6$) that is determined by DFT. The critical alkyl chain length causes the instability of TFSI^- at $x=6$, which influences the propanol isomer effect in the mixed system.

Acknowledgements

We appreciate Dr. T. Takekiyo and Dr. M. Aono of National Defense Academy for helpful discussions.

Appendix A. Supplementary data

Supplementary material related to this article can be found, in the online version, at doi:10.1016/j.cplett.2014.09.003.

References

- [1] L.A. Blanchard, D. Hancu, E.J. Beckman, J.F. Brennecke, *Nature* 399 (1999) 28.
- [2] J.F. Brennecke, B.E. Gurkan, *J. Phys. Chem. Lett.* 1 (2010) 3459.
- [3] M.Z. Ertem, S.J. Konezny, M. Araujo, V.S. Batista, *J. Phys. Chem. Lett.* 4 (2013) 745.
- [4] R. Babarao, S. Dai, D. Jiang, *J. Phys. Chem. B* 115 (2014) 9789.
- [5] J. Tang, H. Tang, W. Sun, H. Plancher, M. Radosza, Y. Shen, *Chem. Commun.* (2005) 3325.
- [6] H. Katayanagi, K. Nishikawa, H. Shimozaki, K. Miki, P. Westh, Y. Koga, *J. Phys. Chem. B* 108 (2004) 19451.
- [7] E.J. González, L. Alonso, A. Domínguez, *J. Chem. Eng. Data* 51 (2006) 1446.
- [8] K. Sahandzhieva, D. Tuma, S. Breyer, A. Pérez-Salado Kamps, G. Maurer, *J. Chem. Eng. Data* 51 (2006) 1516.
- [9] U. Dománska, L.M. Casás, *J. Phys. Chem. B* 111 (2007) 4109.
- [10] J.R. Trindade, Z.P. Visak, M. Blesic, I.M. Marrucho, J.A.P. Coutinho, J.N.C. Lopes, J. Rebelo, *J. Phys. Chem. B* 111 (2007) 4737.
- [11] R. Ferreira, M. Blesic, J. Trindade, I. Marrucho, J.N. Canongia Lopes, L.P.N. Rebelo, *Green Chem.* 10 (2008) 918.
- [12] J. Gmehling, *Pure Appl. Chem.* 75 (2003) 875.
- [13] Z. Lei, B. Chen, C. Li, H. Liu, *Chem. Rev.* 108 (2008) 1419.
- [14] R.L. Gardas, J.A.P. Coutinho, *Fluid Phase Equilib.* 266 (2008) 195.
- [15] J. Rarey, J. Gmehling, *Pure Appl. Chem.* 81 (2009) 1745.
- [16] R.S. Santiago, G.R. Santos, M. Aznar, *Fluid Phase Equilib.* 295 (2010) 93.
- [17] R.S. Santiago, M. Aznar, *Fluid Phase Equilib.* 303 (2011) 111.
- [18] R.S. Santiago, G.R. Santos, M. Aznar, *Fluid Phase Equilib.* 278 (2009) 54.
- [19] R.S. Santiago, G.R. Santos, M. Aznar, *Fluid Phase Equilib.* 293 (2010) 66.
- [20] J. Jacquemin, et al., *Chem. Phys. Chem.* 13 (2012) 1825.
- [21] P.J. Carvalho, V.H. Álvarez, I.M. Marrucho, M. Aznar, J.A.P. Coutinho, *J. Supercrit. Fluids* 52 (2010) 258.
- [22] K. Fujii, T. Fujimori, T. Takamuku, R. Kanzaki, Y. Umebayashi, S. Ishiguro, *J. Phys. Chem. B* 110 (2006) 8179.
- [23] K. Fujii, et al., *J. Phys. Chem. B* 112 (2008) 4329.
- [24] J.C. Lassègues, J. Grondin, R. Holomb, P. Johansson, *J. Raman Spectrosc.* 38 (2007) 551.
- [25] Y. Yoshimura, T. Takekiyo, Y. Imai, H. Abe, *J. Phys. Chem. C* 116 (2012) 2097.
- [26] A.R. Choudhury, N. Winterton, A. Steiner, A.I. Cooper, K.A. Johnson, *CrystEngComm* 8 (2006) 742.
- [27] T.C. Penna, L.F.O. Faria, J.R. Matos, M.C.C. Ribeiro, *J. Chem. Phys.* 138 (2013) 104503.
- [28] X. Shao, W. Schröer, B. Rathke, *J. Chem. Eng. Data* 59 (2014) 225.
- [29] V.R. Vale, S. Will, W. Schröer, B. Rathke, *Chem. Phys. Chem.* 13 (2012) 1860.
- [30] V.R. Vale, B. Rathke, S. Will, W. Schröer, *J. Chem. Eng. Data* 56 (2011) 4829.
- [31] J. Łachwa, P. Morgado, J.M.S.S. Esperancá, H.J.R. Guedes, J.N.C. Lopes, L.P.N. Rebelo, *J. Chem. Eng. Data* 51 (2006) 2215.
- [32] H. Abe, T. Mori, R. Abematsu, Y. Yoshimura, N. Hatano, Y. Imai, J. Kishimura, *J. Mol. Liquids* 167 (2012) 40.
- [33] O. Russina, et al., *J. Phys.: Condens. Matter* 21 (2009) 424121.
- [34] J.D. Holbrey, W. Matthew Reichert, R.D. Rogers, *Dalton Trans.* (2004) 2267.
- [35] G. Raabe, J. Köhler, *J. Chem. Phys.* 129 (2008) 144503.
- [36] A.D. Becke, *J. Chem. Phys.* 98 (1993) 5648.
- [37] C. Lee, W. Yang, R.G. Parr, *Phys. Rev. B* 37 (1988) 785.
- [38] M.W. Schmidt, et al., *J. Comput. Chem.* 14 (1993) 1347.
- [39] A. Merzougui, A. Hasseine, A. Kabouche, M. Korichi, *Fluid Phase Equilib.* 309 (2011) 161.
- [40] A. Fredenslund, R.L. Jones, J.M. Prausnitz, *AIChE J.* 21 (1975) 1086.